AMERICAN SOCIETY FOR MICROBIOLOGY | Journal of Virology®

VIRUS-CELL INTERACTIONS

Functional Analysis of the Dengue Virus Genome Using an Insertional Mutagenesis Screen

Jeffrey W. Perry,[a] Yanhua Chen,[a] Elizabeth Speliotes,[a] Andrew W. Tai[a,b,c]

[a]Division of Gastroenterology, Department of Internal Medicine, University of Michigan Medical School, Ann Arbor, Michigan, USA

[b]Department of Microbiology and Immunology, University of Michigan, Ann Arbor, Michigan, USA

[c]Medicine Service, Ann Arbor Veterans Administration Health System, Ann Arbor, Michigan, USA

ABSTRACT In the last few decades, dengue virus, an arbovirus, has spread to over 120 countries. Although a vaccine has been approved in some countries, limitations on its effectiveness and a lack of effective antiviral treatments reinforce the need for additional research. The functions of several viral nonstructural proteins are essentially unknown. To better understand the functions of these proteins and thus dengue virus pathogenesis, we embarked on a genomewide transposon mutagenesis screen with next-generation sequencing to determine sites in the viral genome that tolerate 15-nucleotide insertions. Using this approach, we generated support for several published predicted transmembrane and enzymatic domains. Next, we created 7 mutants containing the 15-nucleotide insertion from the original selection and found 6 of them were capable of replication in both mammalian and mosquito tissue culture cells. Interestingly, one mutation had a significant impairment of viral assembly, and this mutation may lead to a better understanding of viral assembly and release. In addition, we created a fully infectious virus expressing a functionally tagged NS4B protein, which will provide a much-needed tool to elucidate the role of NS4B in viral pathogenesis.

IMPORTANCE Dengue virus is a mosquito-borne virus distributed in tropical and subtropical regions globally that can result in hospitalization and even death in some cases. Although a vaccine exists, its limitations and a lack of approved antiviral treatments highlight our limited understanding of dengue virus pathogenesis and host immunity. The functions of many viral proteins are poorly understood. We used a previously published approach using transposon mutagenesis to develop tools to study these proteins' functions by adding insertions randomly throughout the viral genomes. These genomes were transferred into cells, and infectious progeny were recovered to determine sites that tolerated insertions, as only the genomes that tolerated insertions would be able to propagate. Using these results, we created viruses with epitope tags, one in the viral structural protein Capsid and one in the viral nonstructural protein NS4B. Further investigation of these mutants may elucidate the roles of Capsid and NS4B during dengue virus infections.

KEYWORDS Capsid, NS4B, dengue virus, mutagenesis, transposon, virus assembly, virus replication

Dengue virus (DENV) is estimated to infect 390 million people worldwide each year (1). In addition, it is suggested that over 3.9 billion individuals in 128 countries are at risk for infection (2), resulting in approximately 1 million hospitalizations and 50,000 deaths annually. Mortality rates may be increased in areas with limited health care resources (3, 4). To date, four serotypes of DENV have been described. Although each serotype most likely once circulated in geographically distinct regions, currently all four

Received 30 November 2017 **Accepted** 3 January 2018

Accepted manuscript posted online 10 January 2018

Citation Perry JW, Chen Y, Speliotes E, Tai AW. 2018. Functional analysis of the dengue virus genome using an insertional mutagenesis screen. J Virol 92:e02085-17. https://doi.org/10.1128/JVI.02085-17.

Editor Michael S. Diamond, Washington University School of Medicine

Address correspondence to Andrew W. Tai, andrewwt@umich.edu.

serotypes cocirculate in Asia, Africa, and the Americas (5). Although a tetravalent DENV vaccine has received regulatory approval in a number of countries, unresolved issues include possibly uneven protection against the different DENV serotypes, a requirement for prior DENV exposure for optimal immunity, and possible increased severity of DENV infection among young children (6–10). Additionally, the lack of approved antiviral treatments underscores the need for specific treatment options, which require a better understanding of DENV pathogenesis.

DENV is a positive-strand RNA virus from the family *Flaviviridae*. The RNA genome consists of 5′ and 3′ untranslated regions flanking a single open reading frame encoding a polyprotein. Cleavage of this polyprotein by the viral NS3 protease, as well as host proteases, releases 10 viral proteins (Capsid [Cap], pre-Membrane [prM], Envelope, NS1, NS2A, NS2B, NS3, NS4A, NS4B, and NS5), which then subvert the host cell to replicate the viral genome and produce progeny virus (11, 12). The functions of several of these proteins, including NS4B, are poorly understood.

To elucidate the functions of viral proteins and their interactions with the host, we sought to determine sites across the DENV genome that tolerate randomly placed 15-nucleotide (nt) insertions with the goal of identifying sites that tolerate functional tags. A powerful tool to characterize protein function has been the use of functional tagging, including epitope tags, fluorescent proteins, and enzymes. However, the highly compact genomes of positive-strand RNA viruses generally do not tolerate insertions, and random tagging is most often lethal to the virus. By using whole-genome transposon insertional mutagenesis, we overcame these challenges by simultaneously screening a library of insertions at every position and determining tolerated positions by passaging the virus. Genomes bearing insertions within intolerant sites were lost, while tolerant sites were selected and amplified. Next, we used next-generation sequencing (NGS) to identify these insertion-tolerant sites by comparing passaged virus to the input RNA. We evaluated our findings by examining insertion tolerance at known functional viral domains, including transmembrane domains and catalytic domains. In addition, we reengineered seven mutants containing the original 15-nucleotide insertion and determined that six grew similarly to the wild type (WT) in Vero and C6/36 mosquito larval cell lines. Interestingly, one Capsid protein mutant could replicate in cells but failed to passage onto naive cells. In addition, we were able to generate and validate an infectious epitope-tagged NS4B mutant in both mosquito and mammalian cells.

RESULTS

Screening the dengue virus genome for tolerated insertions. We conducted a transposon mutagenesis screen on the serotype 2 DENV strain 16681 (Fig. 1). Due to toxicity and instability of the full-length DENV cDNA genome in *Escherichia coli*, we created three subgenomic fragments using the unique SacI, NarI, EcoRV, and XbaI restriction enzyme sites. The resulting fragments contained the first 3,659 nucleotides (fragment A), nucleotides 3660 to 4331 (fragment B), and nucleotides 4332 to 10723 (fragment C). When expressed individually, these three subgenomic clones did not inhibit *E. coli* growth and were genetically stable (data not shown). The subgenomic fragments were subjected to MuA transposase-mediated insertional mutagenesis with a sequence including an antibiotic resistance gene flanked by modified inverted repeats of the bacteriophage Mu right-end sequence engineered to contain a NotI site. The MuA transposase randomly inserted this linear DNA sequence into the plasmids containing the subgenomic DENV fragments. The mutagenized fragment libraries were then cloned back into unmutagenized vectors with antibiotic selection to ensure only the DENV fragments contained the inserted sequence and not the vector backbone. The bulk of the inserted sequence was then excised by NotI digestion and intramolecular ligation to leave a 15-nucleotide insertion at a random site within the subgenomic DENV fragment. This insertion consisted of 8 nucleotides from the NotI site (GCGGCCGC), two flanking nucleotides (boldface) (**T**GCGGCCGC**A**), and a duplication of the 5 nucleotides [N_1 to N_5] directly 5′ of the insertion point ($N_1N_2N_3N_4N_5$TGCGGCCG

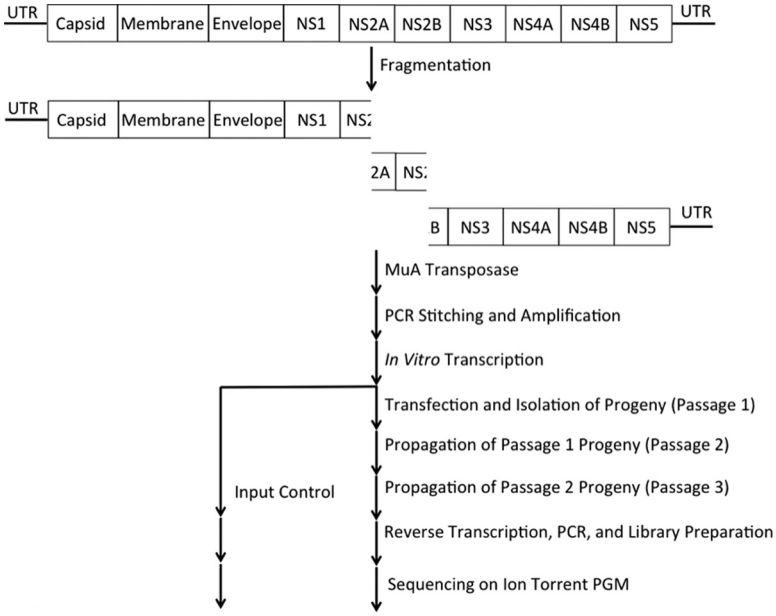

FIG 1 Transposon mutagenesis selection protocol. To avoid genetic instability and toxicity of the full-length DENV cDNA in *E. coli*, we fragmented the genome into three segments that were individually nontoxic and genetically stable. Fifteen-nucleotide insertions were randomly inserted into these three fragments of the DENV genome using MuA transposase and molecular-cloning techniques. The full-length viral genome was reconstructed by PCR and transcribed into viral RNA *in vitro*. Viral RNA mutant libraries were then transfected into permissive Vero cells. Only virus genomes that tolerated the insertion were able to replicate and produce progeny, while viruses that could not tolerate the insertion were nonviable. After 3 days, the progeny viruses were collected from the culture supernatant. Half were used to infect naive cells, while the other half were sequenced. This was repeated twice more to obtain passage 2 and passage 3 viruses. Progeny viral RNA was recovered and reverse transcribed into viral cDNA. The viral cDNA was PCR amplified into 400-bp products and used to create a sequencing library for the Ion Torrent PGM sequencing platform. An input control of the viral RNA from the original transfection was also reverse transcribed, PCR amplified, and made into sequencing libraries. UTR, untranslated region.

$CAN_1N_2N_3N_4N_5$). This resulted in the addition of 5 amino acids (aa) in one of three reading frames, with a possibility of altering the amino acid immediately 5′ of the inserted sequence but no possibility of creating a stop codon in any reading frame. To estimate the complexity of these libraries, we determined the number of independent colonies from the transformations of these intramolecular digests. We estimated the complexity of the three libraries to be 16.9-fold (fragment A), 33.7-fold (fragment B), and 7.1-fold (fragment C) coverage at the nucleotide level.

Using these libraries as templates, full-length DENV genomes with a 5′ T7 RNA promoter sequence were created using splicing overlap extension (SOE) PCR and the corresponding wild-type fragments so that each genome had one insertion. *In vitro*-transcribed viral RNA libraries were than transfected into Vero cells. Three days after the transfection, half of the supernatant was passaged onto naive Vero cells, and the remainder was used to isolate viral RNA. This process was repeated twice more to generate passages 2 and 3.

NGS libraries were created from the original transfected RNA (input), passage 2, and passage 3 for sequencing on the Ion Torrent PGM platform. Raw reads from the Ion Torrent PGM sequencing run were filtered to remove reads lacking a NotI sequence. These reads were then aligned to the DENV genome, and insertion sites were identified and quantitated using Bowtie2 (see Data Set S1 in the supplemental material for the complete data set). Using the NotI only reads, the Lander-Waterman sequencing coverage ranged from 650-fold to 155,344-fold, suggesting that only rare insertions would have been missed (i.e., less than 1 in 650, or about 0.15% frequency). As this calculation uses the entire read length, containing both wild-type and NotI sequences,

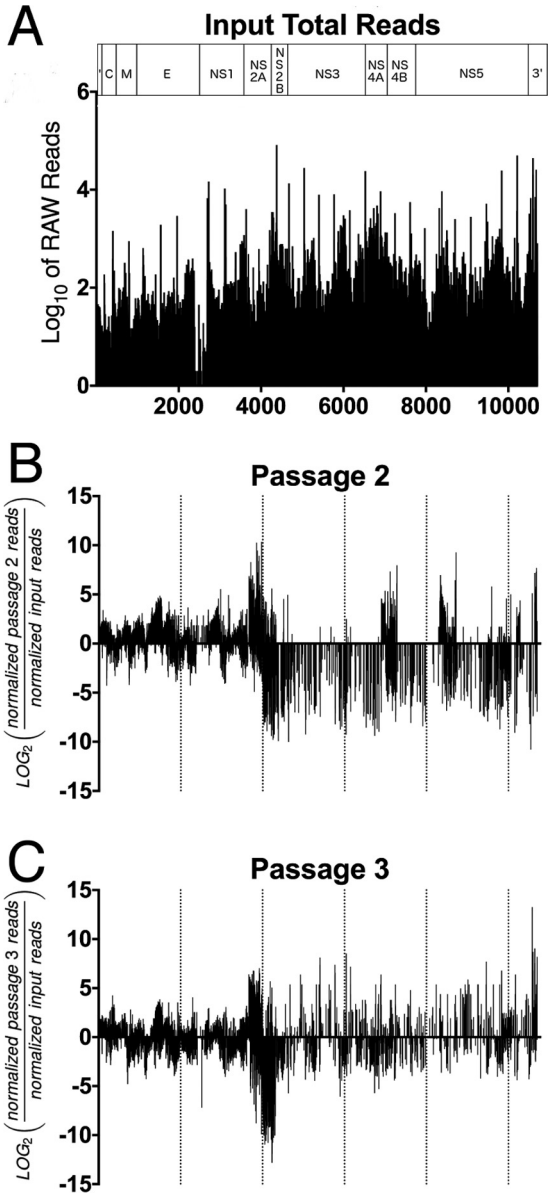

FIG 2 Next-generation sequencing results. (A) Raw sequence reads were filtered for reads that contained a NotI site. The filtered reads were mapped back to the viral genome using Bowtie2, and the insertion site of the transposon was determined and quantitated. Log_{10} filtered reads are plotted on the *y* axis and nucleotide positions on the *x* axis. C, Capsid; M, Membrane; E, Envelope. (B and C) To compare insertions in passaged viral libraries with the input, the number of insertions at each nucleotide position from passage 2 (B) or passage 3 (C) was normalized to the total number of reads from the sequencing run divided by the normalized reads at that nucleotide position from the input and log_2 transformed. These enrichment ratios are plotted on the *y* axis, with nucleotide positions on the *x* axis. Insertion sites that had more reads in the passage 2 or 3 samples than the input have positive values, while insertion sites with fewer reads than the input have negative values.

and therefore overestimates insertional coverage, we also examined the depth of identified NotI insertion sites. By this analysis, 9,319 of the 10,724 nucleotides (86.9%) of the DENV genome had at least one mapped read containing an insertion (Fig. 2A). When reads containing the NotI insertion from the passage 2 and 3 samples were added, the insertional coverage of our library rose to 10,171 (94.8%), which suggests that only about 5% of the sites in the DENV genome lacked an insertion site in our library. To quantitate enrichment or depletion of insertions at any given site, we first normalized the number of reads per site by the total number of sequencing reads

for the run. The number of normalized reads per site from passage 2 or passage 3 was then divided by the number of normalized input reads and $\log_2$ transformed so that positive numbers indicated enrichment and negative numbers indicated depletion (Fig. 2B and C).

Insertions are generally not enriched in known transmembrane domains or catalytic domains. We examined enrichment and depletion of insertions at sites in the DENV genome with known functions and thus expected to be intolerant of insertions. First, the majority of known or predicted transmembrane domains across the DENV proteins were not enriched for insertions based on comparison of read counts in passage 3 to those in the input (Fig. 3). Interestingly, the transmembrane domain of Capsid and the third predicted domain of NS2A were relatively tolerant of insertions. For example, the average NS2A enrichment ratio was 0.39, while the averages for the five predicted transmembrane domains were −0.19, 0.22, 1.24, −0.37, and −3.29. Second, the catalytic domains of both NS3 (average ratio, −0.26; nt 4428 to 4959) and NS5 (average ratio, −0.02; nt 9060 to 9507) were not enriched for insertions (Fig. 4), nor was the fusion peptide of Envelope (average ratio, −0.62; nt 1230 to 1269). These findings support the conclusion that regions in the DENV genome that do not tolerate insertions may carry out functions required for the viral life cycle.

Mutants containing a NotI insertion are viable and have growth kinetics similar to that of wild-type DENV in tissue culture cells. To further validate our findings, we reengineered seven highly enriched mutants containing the 15-nt transposon genetic scar in the Capsid, Membrane, NS4A, NS4B, and NS5 genes (Table 1). These sites were chosen based on enrichment of 8-fold or greater in passage 3 compared to the input control and flanking regions of ≥3 nt without depletion. We picked no more than two sites per viral protein. The two Capsid mutants, at nt 106 and 345, occurred at the 2nd amino acid from the N terminus and in the middle of the 4th alpha helix, respectively. The Membrane mutant at nt 785 rests in a site found in the endoplasmic reticulum (ER) lumen close to the first transmembrane domain. The insertion in NS4A at nt 6769 lies in the C-terminal 2-molecular-weight (2K) peptide that is cleaved from NS4A by the viral protease and from NS4B by an unidentified host protease (13). Two NS4B insertions were introduced at nt 6897 in a cytoplasmic domain between the N terminus and the first transmembrane domain and at nt 7281 between the third and fourth transmembrane domains on the ER luminal side. Finally, the mutant in NS5 at nt 9466 is near the C-terminal end of the catalytic domain.

Of the seven recovered mutants, only two mutants (in Capsid and NS5) mapped to regions of DENV proteins with solved structures, while the other insertions were in proteins or regions of proteins without known structures. The solved structure of the DENV Capsid protein (Protein Data Bank [PDB] ID 1SFK) includes the insertion at nt 345, but not the insertion at nt 106 (Fig. 5A and B). The insertion is represented as a yellow sphere and can be observed from the side (Fig. 5A) as well as when looking at the top of the structure (Fig. 5B). The NS5 insertion at nt 9466 lies at surface-exposed residues far from the predicted catalytic site (Fig. 5C).

Mutant viral genomes were transfected into 293T cells, as we found that they are more efficient at recovering virus after transfection than Vero cells. Four of the mutants exhibited growth kinetics that was not significantly different from that of the wild-type virus when 293T cell-derived virus was used to infect Vero cells or the mosquito larval cell line C6/36. Two mutants had slight delays in replication indicated by small but significant decreases in titers at 72 and 120 h postinfection, but not at 168 h. Interestingly, these mutants had replication delays in either C6/36 (6897 NS4B) or Vero (106 Capsid) cells, but not in both (Fig. 6). One Capsid insertion at nt 345 replicated in 293T cells and caused cytopathic effect in those cells but did not produce viral plaques and therefore was not analyzed by plaque assay.

Membrane association of Capsid mutants. Our selection data suggested that the transmembrane domain of Capsid tolerated insertions. Capsid contains a single transmembrane signal peptide that mediates the translocation of prM into the endoplasmic

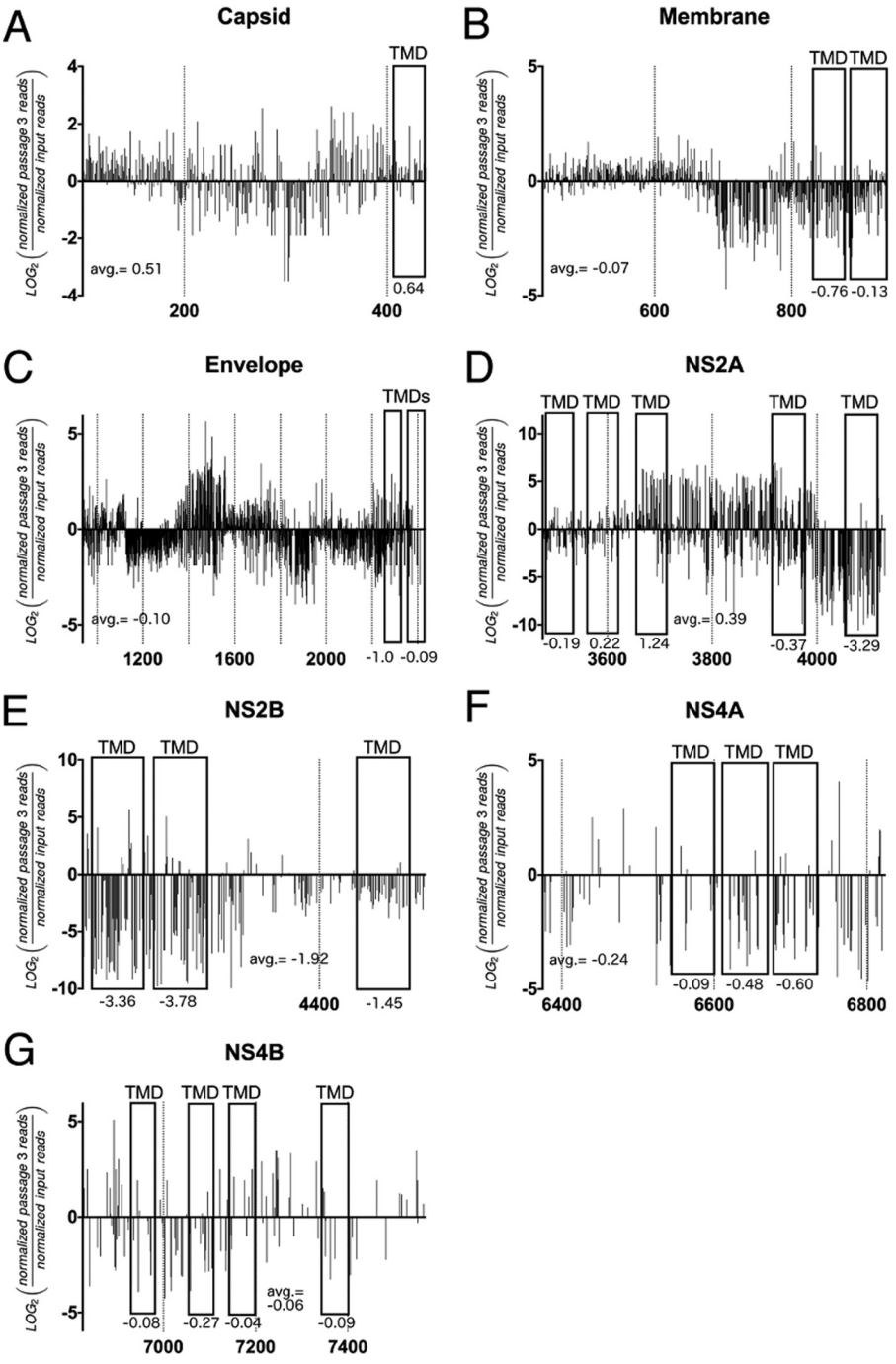

FIG 3 Tolerance of predicted transmembrane domains (TMDs) for insertions. Enrichment ratios for Membrane, Envelope, NS2A, NS2B, NS4A, and NS4B are plotted on the *y* axis, with nucleotide positions on the *x* axis. Known or predicted transmembrane domains in each protein are boxed. Also indicated are the average enrichment ratios for the entire protein and for each transmembrane domain.

reticulum. This transmembrane domain is then cleaved by the viral protease NS2B/NS3 to release the functional cytosolic form (reviewed in reference 14). We generated an expression vector encoding wild-type Capsid, as well as the insertions 106 Capsid NotI, 345 Capsid NotI, and the most enriched insertion within the Capsid transmembrane domain at nt 420. Although the 106 Capsid NotI mutant was mildly attenuated in Vero cells and the 345 Capsid NotI mutant failed to propagate, both proteins were expressed to levels similar to wild type and associated with cellular membranes (Fig. 7). Although

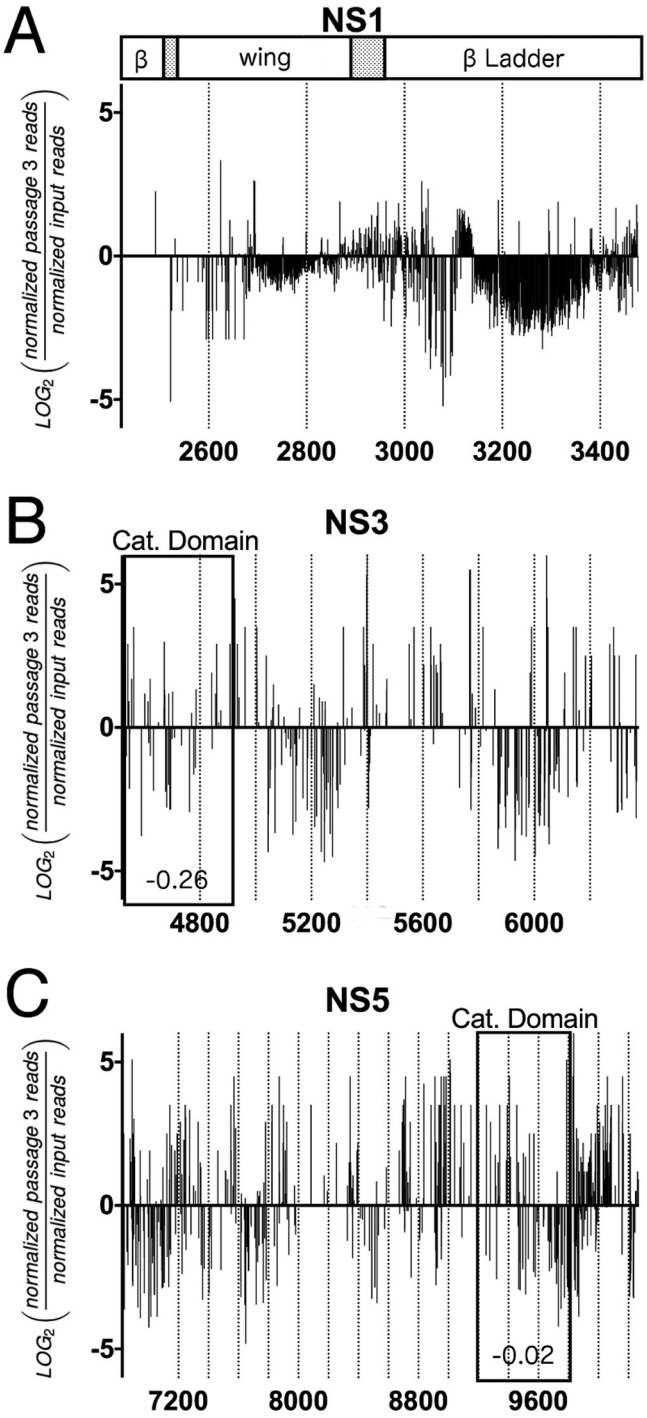

FIG 4 Tolerance of insertions in NS1, NS3, and NS5. (A) Enrichment ratios in the sequence coding for NS1 are plotted on the *y* axis, with nucleotide positions on the *x* axis. A schematic of the proposed structure of NS1 is included at the top of the graph, where the shaded boxes represent the connector regions flanking the wing domain. (B and C) Enrichment ratios in the sequences coding for NS3 (B) and NS5 (C) are plotted on the *y* axis, with nucleotide positions on the *x* axis. Catalytic (Cat.) domains are boxed. Also indicated are the enrichment ratios for the predicted catalytic domains, which are also boxed.

the 420 Capsid NotI mutant had lower protein levels than wild-type Capsid, it still associated with cellular membranes. As a control, we transiently expressed the soluble protein green fluorescent protein (GFP) in 293T cells, followed by fractionation as for Capsid proteins; as expected, the soluble GFP was detected only in the soluble fraction (Fig. 7).

TABLE 1 NotI-containing dengue virus mutation insertion sites[a]

Site	Wild-type nucleic acid sequence	Insertion nucleic acid sequence	Wild-type amino acid sequence	Insertion amino acid sequence	Insertion length (nt/aa)
106 (Capsid)	ATAAC_CAACG	ATAACTGCGGCCGCAATAACCAACG	NNQR	NNCGRNNQR	15/5
345 (Capsid)	AGAGG_GTTCA	AGAGGTGCGGCCGCAAGAGGGTTCA	RGFR	RGAAARGFR	15/5
785 (Membrane)	AGGGG_CCTGG	AGGGGTGCGGCCGCAAGGGGCCTGG	EGAW	EGVRPQGAW	15/5
6769 (NS4A)	AAGAC_AACCA	AAGACTGCGGCCGCAAAGACAACCA	QDNQ	QDCGRKDNQ	15/5
6897 (NS4B)	CCCGA_GAGCA	CCCGATGCGGCCGCACCCGAGAGCA	PESN	PDAAAPESN	15/6
7281 (NS4B)	ACAGT_GATTG	ACAGTTGCGGCCGCAACAGTGATTG	TVID	TVAAATVID	15/5
9466 (NS5)	GCATT_CAGCA	GCATTTGCGGCCGCAGCATTCAGCA	SIQH	SICGRSIQH	15/5

[a]Underlining indicates the inserted nucleotides or amino acids in each mutant.

Recovery of a viable dengue virus mutant expressing HA-tagged NS4B. We next introduced hemagglutinin (HA) or FLAG epitope tags into the sites that tolerated the original NotI-containing insertions. Unfortunately, we were unable to recover virus tagged with HA or FLAG in the majority of these sites. To date, we have recovered one functionally tagged infectious virus encoding an HA epitope tag at nt 6897 in NS4B, which is a multipass transmembrane domain protein. This HA tag is predicted to be located at the N-terminal end of NS4B before the first transmembrane domain and on the cytosolic side of the membrane (Fig. 8A). This functionally tagged virus replicated in Vero and C6/36 cells with kinetics similar to that of the wild-type parental strain throughout a 7-day time course (Fig. 8B and C) and produced plaques similar in size to those of the wild type in a plaque assay (data not shown). The HA-tagged NS4B protein could be observed by Western blotting in 293T, Vero, and C6/36 cells (Fig. 8D). Interestingly, immunoblotting of infected C6/36 cells with anti-HA antibody revealed two bands not seen in uninfected C6/36 cells or in infected human cells. Treatment of C6/36 lysates with the enzyme peptide-*N*-glycosidase F (PNGase F), which removes N-linked glycans, did not affect the migration of the two bands, suggesting that neither represents a glycosylated form of NS4B (data not shown). In addition, we were able to immunoprecipitate HA-NS4B with anti-HA antibodies (Fig. 8E). To investigate whether viability of the HA insertion requires secondary mutations, we subjected the 6897 NS4B HA strain originally isolated from transfection to Sanger sequencing and discovered seven mutations. Six of the mutations were silent, with only a mutation at nt 6981 causing an amino acid change from leucine to phenylalanine. We then repeated the experiment in triplicate and sequenced the progeny viruses. No mutations were observed at nt 6981. The three independent viral preparations of 6897 NS4B HA had growth curves in Vero cells similar to those of the wild-type virus, demonstrating that the L6981F substitution observed in the original experiment is not required for recovery

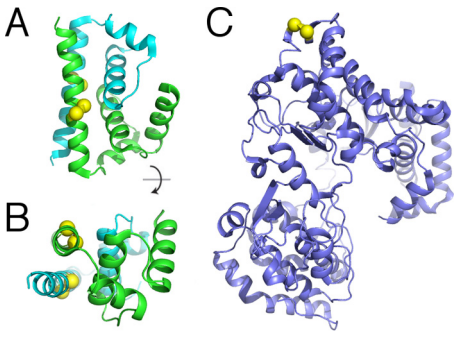

FIG 5 Three-dimensional models of Capsid and NS5 revealing that tolerated insertion mutants are in exposed regions. Three-dimensional models of the DENV proteins Capsid (PDB ID 1SFK) (A and B) and NS5 (PDB ID 3P8Z) (C) were generated using the PyMOL molecular graphics system (version 1.8; Schrödinger, LLC). Only two insertion mutants were observed in regions of structural certainty, while the other insertion mutants were in proteins or protein regions without solved structures. All insertions, represented as yellow spheres, are on exposed sites of the protein and can be observed from the side (A and C) or from the top (B) of the protein.

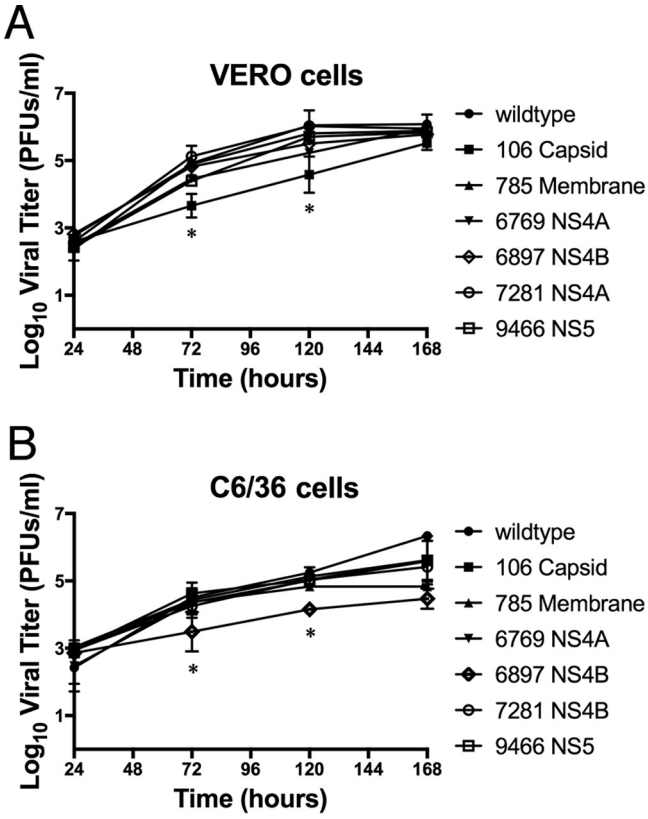

FIG 6 Validation of insertion mutants in Vero and C6/36 mosquito larval cells. Six sites in the viral genome that tolerated insertions were individually mutagenized to recapitulate the original observed insertions. Vero cells (A) or the mosquito larval cell line C6/36 (B) was infected with the indicated viruses for 7 days at an MOI of 0.05 PFU/cell, and titers were determined by plaque assay. *, $P < 0.05$. The error bars represent standard errors of the results of at least three independent experiments with at least two technical replicates per condition.

or propagation of the 6897 NS4B HA mutant. We passaged the 6897 NS4B HA mutant over four passages and 20 days in 293T cells and sequenced the insertion after each passage to confirm that it remained genetically stable (Fig. 8F). Finally, we performed double-label immunofluorescence and found colocalization of anti-HA and anti-NS4B signals in cells infected with the 6897 NS4B HA-tagged virus (Fig. 9). Recovery of the 6897 NS4B HA mutant demonstrates the feasibility of using this transposon-mapping strategy to identify candidate sites for functional tagging, which could be valuable for the generation of additional tagged mutants.

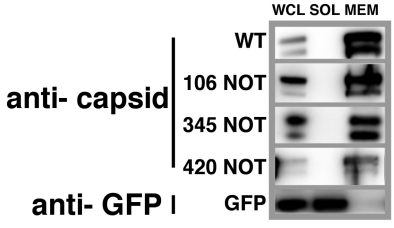

FIG 7 Transient expression of DENV Capsid associates with membranes. Expression plasmids encoding WT or mutant (106 NOT, 345 NOT, or 420 NOT) full-length DENV Capsid (aa 100 to 438) or GFP were transiently transfected into 293T cells 48 h before the cells were harvested and boiled in sample buffer to prepare whole-cell lysate (WCL) or homogenized and subjected to ultracentrifugation to isolate a membrane pellet. WCL, soluble protein (SOL), and membrane-bound protein (MEM) were separated by SDS-PAGE and subjected to Western blotting for the indicated proteins.

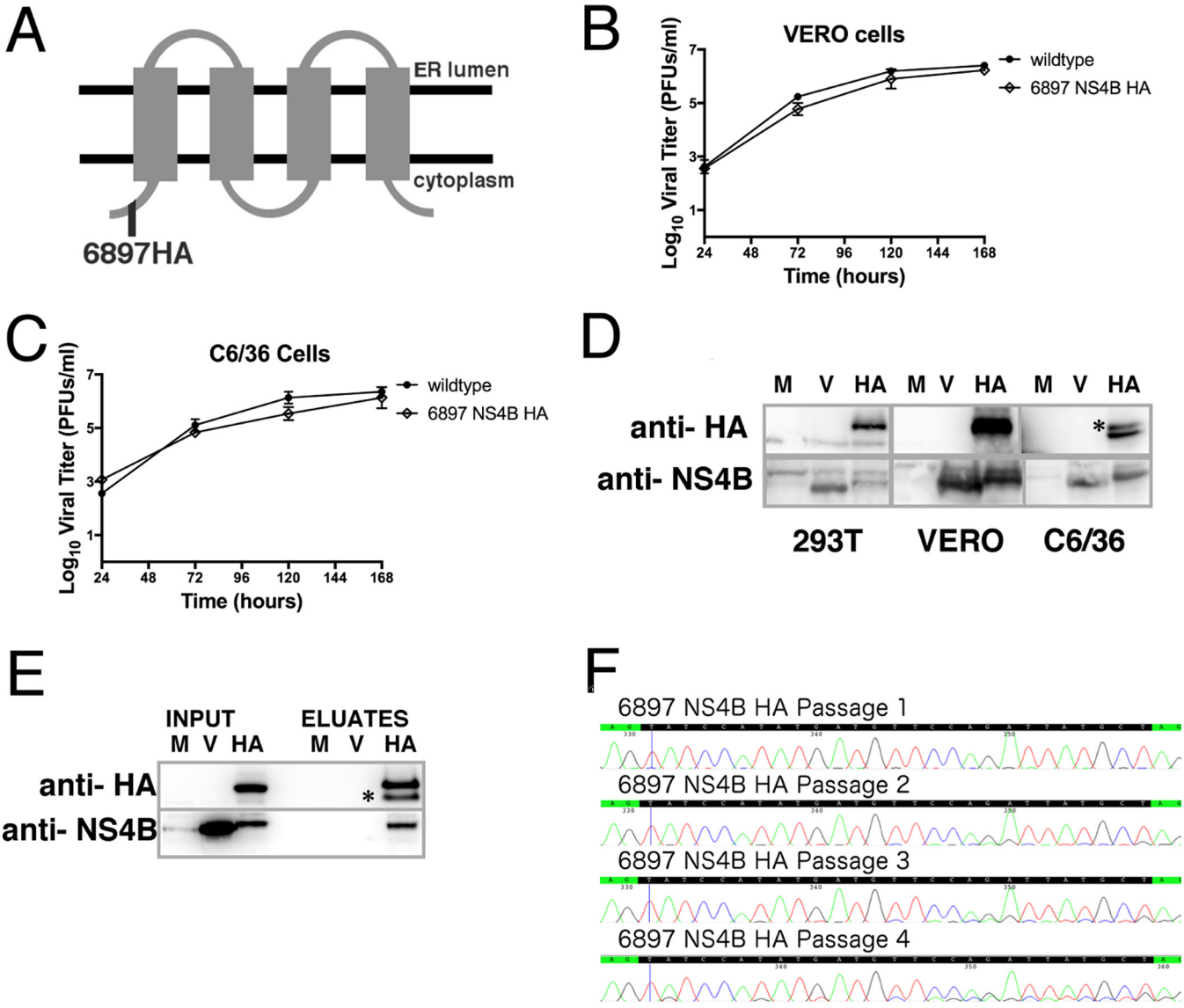

FIG 8 Characterization of the 6897 NS4B HA mutant. (A) Predicted topology of the NS4B protein with the location of the HA epitope tag at nt 6897 indicated. (B and C) Vero (B) or C6/36 (C) cells were infected with virus for 7 days at an MOI of 0.05 PFU/cell, and titers were determined by plaque assay. The error bars represent standard errors of the results of at least three independent experiments with at least two technical replicates per condition. (D) Vero, 293T, or C6/36 cells were mock infected (M) or infected with wild-type DENV (V) or 6897 NS4B HA (HA) for 5 days and analyzed via Western blotting with anti-NS4B or anti-HA. A small difference between the apparent molecular masses of wild-type NS4B (~25 kDa) and HA-tagged NS4B (~26 kDa) could be detected. (E) Immunoprecipitation of HA-NS4B from lysates of Vero cells infected for 5 days with the wild type (V) or 6897 NS4B HA (HA) at an MOI of 0.05 or mock infected (M). Samples were analyzed by Western blotting with the indicated antibodies. An additional HA-reactive band was immunoprecipitated from 6897 NS4B HA-infected cells (asterisk). (F) To test the genetic stability of the 6897 NS4B HA mutation, the virus was passaged on Vero cells four times at an MOI of 0.05 for 5 days each time, and the HA insert was sequenced by Sanger sequencing. HA insertion sequence is indicated in black flanked with wild-type sequence indicated in green.

Dengue virus mutant 345 Capsid is defective at progeny assembly. The 345 Capsid NotI mutant selected from this screen did not infect naive cells; this site was not located in the transmembrane domain or near either cleavage site (Fig. 5 and 10A). Mutants with insertion of either NotI or HA at this position could replicate to wild-type levels after viral RNA transfection, and the replication could be inhibited by the viral polymerase inhibitor 2′-*C*-methyladenosine (2′-CMeA) (Fig. 10B). In addition, viral genomes were detectable in the cell supernatant after viral RNA transfection, although at an approximately 10-fold lower titer than the wild type. To test whether a lipid membrane protected these secreted genomes, we subjected the cell culture supernatant to nuclease treatment in the presence or absence of detergent. Interestingly, the

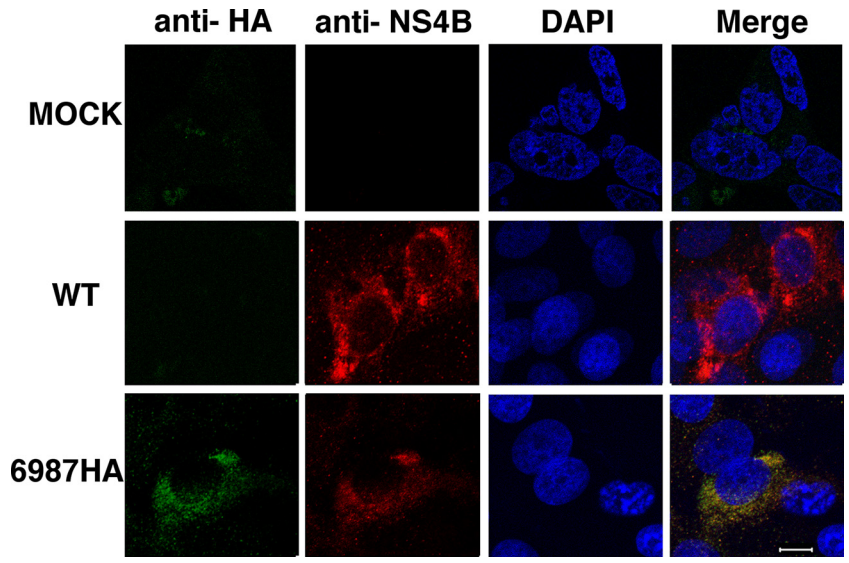

FIG 9 Confocal microscopy of the 6897 NS4B HA mutant. Vero cells were infected with WT or 6897 NS4B HA (6897HA) at an MOI of 0.05 or mock infected (Mock). At 5 days postinfection, the cells were fixed and dual stained with anti-HA (green) and anti-NS4B (red), as well as DAPI (blue). Bar, 10 μm.

secreted viral genomes were nuclease sensitive only in the presence of detergent, indicating that they were contained in membrane structures (Fig. 10C). To check if the DENV genome was secreted from replicon-bearing cells, we assayed the supernatant from these cells and found no secreted genomes above background (data not shown). Although the 345 Capsid mutants could replicate and secrete protected viral genomes, the secreted genomes were unable to infect naive cells (Fig. 10D). As recovery of viruses from the screen requires production of infectious virus, we hypothesized that this mutant may have been *trans*-complemented by wild-type Capsid protein during library selection. We tested this possibility by transfecting viral RNA into 293T cells, followed by transient expression of WT Capsid or GFP. Seven days after the transfection, the culture medium was passaged onto naive cells. After 5 days of infection, total cellular RNA was harvested and viral genomes were quantitated by quantitative reverse transcription (qRT)-PCR. Transfection of wild-type Capsid, but not GFP, into infected cells could rescue the 345 mutant's propagation (Fig. 10E). Interestingly, transfection of wild-type Capsid into cells expressing 345 Capsid NotI genomes also significantly increased the number of secreted viral genomes in the culture medium. Finally, expression of the HA-tagged Capsid in RNA-transfected cells was detectable by immunoblotting (Fig. 10F).

DISCUSSION

A major barrier to our understanding of DENV pathogenesis is our limited understanding of the functions of several of its proteins. Functional tagging of proteins at arbitrary sites can have significant drawbacks (reviewed in reference 15). Moreover, positive-strand RNA viral genomes are compact, with most proteins having multiple functions, and thus arbitrary tagging is most often lethal.

In an attempt to define sites in the viral genome that would tolerate small insertions by an unbiased method, we used a genomewide transposon mutagenesis screen with NGS. Sites that were not enriched for insertions included previously studied viral protein domains, including predicted transmembrane domains, the fusion peptide of Envelope, and catalytic domains of NS3 and NS5. Many other regions of the viral genome with no known structure or function were also intolerant of insertions. These sites could be critical for correct RNA or protein folding, encode unknown protein functions, or mediate interactions with other viral or host proteins.

A transposon mutagenesis strategy has been employed for a number of other RNA

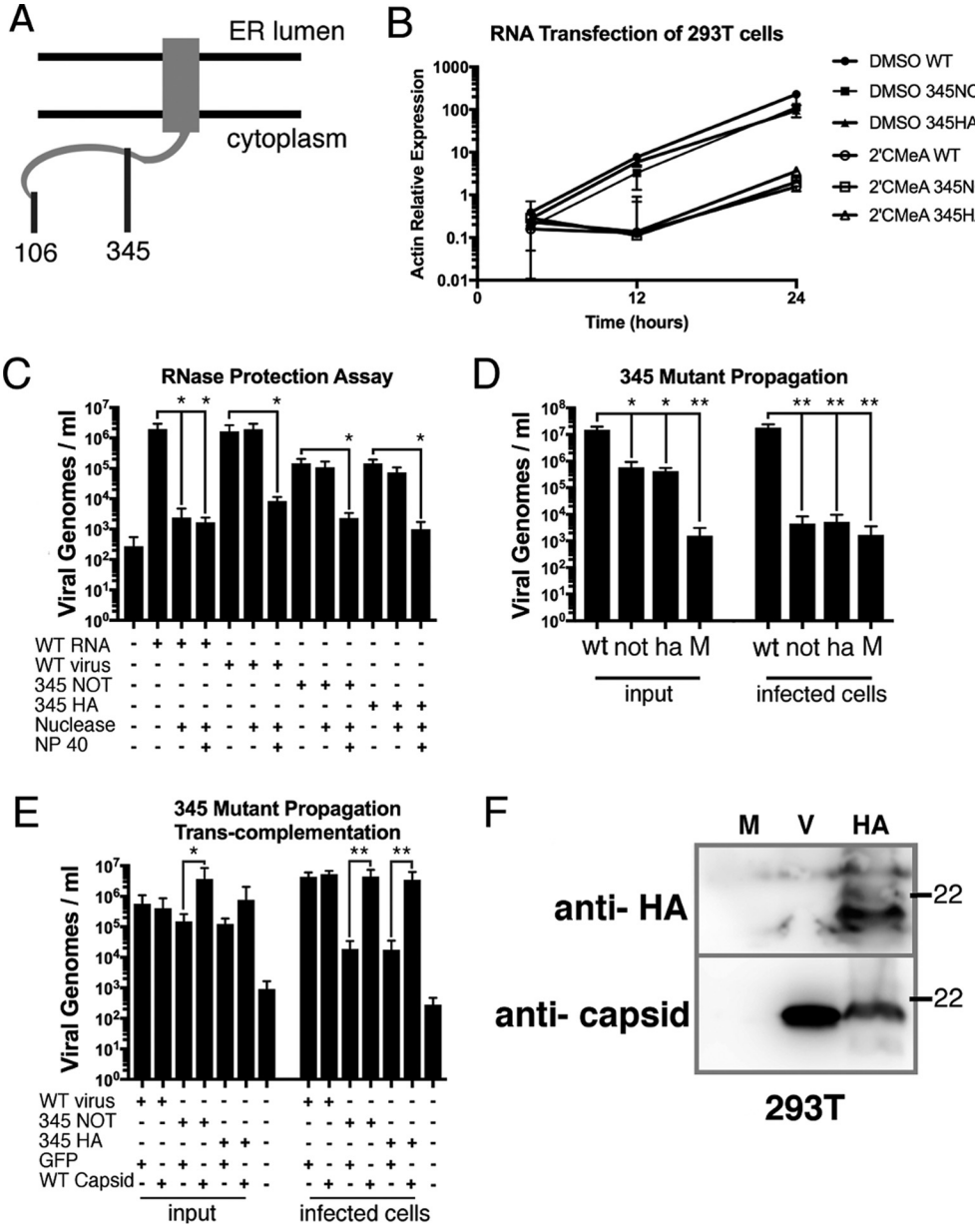

FIG 10 Characterization of the 345 Capsid mutant. (A) Schematic of Capsid protein with insertions at sites 106 and 345 indicated. (B) 293T cells were transfected with WT, 345 Capsid NotI (345 NOT), or 345 Capsid HA (345 HA) viral RNA; the medium was replaced with dimethyl sulfoxide (DMSO) or 1 μM 2′-CMeA (polymerase inhibitor); and viral genomes were quantified 4, 12, or 24 h posttransfection. (C) 293T cells were transfected with WT, 345 Capsid NotI (345 NOT), or 345 Capsid HA viral RNA (345 HA), and secreted viral genomes were harvested 7 days after transfection. The secreted genomes were nuclease treated in the presence or absence of detergent and quantitated by qRT-PCR. (D) Secreted viral genomes were harvested 7 days after transfection (input) and used to infect naive 293T cells (infected cells). After 5 days, whole cellular RNA from the infected naive cells was harvested, and viral genomes were quantitated by qRT-PCR. M, mock infected. (E) 293T cells were transfected with viral RNA and then transfected the following day with either a wild-type Capsid- or a GFP-expressing plasmid. Seven days after transfection, secreted viral genomes were harvested (input) and used to infect naive cells (infected cells). After 5 days, whole cellular RNA from the infected naive cells was harvested, and viral genomes were quantitated by qRT-PCR. (F) 293T cells were transfected with the indicated viral genomes (Mock [M], wild type [V], or 345 Capsid HA [HA]), and the lysates were subjected to immunoblotting with the indicated antibodies. *, $P < 0.05$; **, $P < 0.005$. The error bars represent standard errors of the results of at least three independent experiments with at least two technical replicates per condition.

viruses (16, 17), including Venezuelan equine encephalitis virus (18), hepatitis C virus (19, 20), and Zika virus (21). One goal of these studies has also been to identify sites in the viral genome that tolerate functional tags. One recurring observation from these screens is the apparent intolerance of most sites for insertions. However, we hypoth-

esize that this large reduction in recovered insertion mutants is also due in part to bottlenecks during initial RNA transfection and subsequent passaging. For these studies, viral RNA is transfected or electroporated into cells, allowed to infect, and then passaged onto naive cells. These rounds of infection create bottlenecks that may artificially reduce the number of independent viruses that are recovered. To try to overcome this issue, we used significantly more replicates during the selection process than other published endeavors, using a pool of 18 (fragments A and C) or 9 (fragment B) independent transfections.

Interestingly, there were two predicted transmembrane domains that did not strongly select against insertions: the transmembrane domain of Capsid and the third predicted transmembrane domain of NS2A. The predicted transmembrane domains of NS2A have not been validated biochemically or structurally (22). Our results do not fully support the previous prediction of 5 transmembrane domains in NS2A, as the third predicted transmembrane domain did not strongly select against insertions. A recent paper has suggested that the NS2A protein contains seven transmembrane domains that form a viroporin protein (23). Our data suggest that five of the proposed seven transmembrane domains in that study generally tolerate insertions, and thus, the model in that paper is not supported by our results. Further investigation is needed to understand the topology of NS2A, which could be greatly aided by functionally tagged mutants generated from future experiments. In addition, we found that the most highly enriched insertion within the transmembrane domain did not affect Capsid's association with cellular membranes when expressed in 293T cells, suggesting that the transmembrane domain can tolerate addition of charged amino acids, or possibly that the transmembrane domain is not required for membrane association of full-length Capsid.

We reengineered mutants containing the transposon genetic scar in Capsid, Membrane, NS4A, NS4B, and NS5 viral proteins. Two mutants had slight delays in infection in either Vero (106 Capsid NotI) or C6/36 (6897 NS4N NotI) cells. These mutants may suggest slight differences in the folding or function of these proteins in mosquito versus mammalian cells. However, the fact that all of the generated mutants identified in a mammalian screen were able to productively infect mosquito cells suggests that the six sites probed have similarly nonessential functions in both species.

The insertion site at nt 345 in the Capsid protein clearly has a defect in propagation; *trans*-complementation may have allowed the mutant to be selected for in this screen (24). Indeed, we were able to rescue the 345 Capsid NotI and HA mutants by *trans*-complementation. In any case, this mutant could be a useful tool in understanding DENV assembly. The 345 insertion lies in the α-4 helix, which has been shown to be important for virus assembly (25). Capsid binds to viral RNA and may traffic the genome to sites of virus assembly; how this occurs is poorly understood, but the mutant may help elucidate this step of the viral life cycle (reviewed in reference 14).

Unfortunately, HA or FLAG tags at NotI insertion-tolerant sites were lethal at five of the seven sites tested, most likely due to differences in charge distribution and lengths of insertions. However, one site (nt 6897 in NS4B) did tolerate the addition of a functional HA tag, but not a FLAG or 6×His tag. Another group has also reported the insertion of an HA tag at the N terminus of NS4B before the first transmembrane domain (26, 27). It was used to elucidate the role of DENV NS4B in inducing mitochondrial structure alterations, highlighting the utility of functionally tagged viral proteins to study their functions (27). Although the exact site was not described in either report, our own data suggest that eight sites in this region may tolerate insertions. This previously described HA-NS4B virus reached endpoint titers similar to those of the wild type but displayed slower viral kinetics at earlier time points (24 and 48 h postinfection) in high-multiplicity of infection (MOI) infections. Our 6897 NS4B HA mutant replicates in tissue culture with kinetics similar to that of the wild type at a low MOI, as well as at early time points.

During the preparation of this article, a similar transposon mutagenesis-mapping paper was published for DENV (28) describing the generation of epitope-tagged viruses

with tags inserted into Capsid and NS1. There were a number of differences between the methods used (e.g., cell types, transfection approaches, length of infection of cells before passage, sequencing platforms, and handling of bottlenecks) that could account for the observed differences. One key difference was the insertional coverage of the libraries. The Eyre et al. RNA input library had 43.8% insertional coverage of the genome, which after selection dropped to 10.5% and 9.4%. In contrast, our initial RNA input library contained inserts in 86.9% of the genome, which decreased to 48.1% and 45.7% of the genome after passaging. Comparison of the enriched insertion sites between our two studies revealed significant overlap. Nine of the top 10 most enriched mutants from the Eyre et al. study were tolerated in our own screen, with enrichment ratio values ranging from 1.43 to 2.78 (corresponding to 2.7-fold and 6.9-fold enrichment, respectively). The two mutants that tolerated epitope tags in the Eyre et al. study were also tolerated in our data set, with the nt 403 site having a ratio of 0.97 and the nt 2941 site having a ratio of 2.06. Additionally, comparison of the insertion-tolerant sites within NS1 from the two studies revealed similar tolerance for insertions in the second linker domain and the C-terminal end of the β-ladder. In contrast, only one of the seven NotI mutants reengineered in our study (6897 NS4B NotI) was selected for in the Eyre et al. study. The other mutants may have been lost due to genome coverage and bottleneck effects, as most of their normalized input read counts were low at these sites: 3, 15, 20, 0, 0, and 5 for the mutants 106 Capsid, 345 Capsid, 785 Membrane, 6769 NS4A, 7281 NS4B, and 9466 NS5, respectively. Overall, this suggests that using both data sets as resources could be powerful for further experiments.

This genomewide transposon mutagenesis screen provides a valuable resource by mapping sites in the DENV genome that tolerate short NotI-containing insertions. By coupling NGS to the screen, we have been able to validate seven NotI-containing mutants, as well as two HA-expressing mutants. Further characterization of tolerated insertion sites may lead to the development of additional viable viruses expressing tags in other viral proteins. Finally, generation of tagged mutants in Capsid and NS4B will be a useful tool to elucidate the roles of Capsid and NS4B in viral infection and pathogenesis.

MATERIALS AND METHODS

Cells and viral strains. Vero, 293T, and C6/36 cells were purchased from the American Type Culture Collection (ATCC) and maintained as previously described. Dengue virus serotype 2 strain 16681 expressed as the infectious cDNA clone pD2/IC-30P-NBX was obtained from the Centers for Disease Control and Prevention. The single NotI site in the plasmid upstream of the T7 promoter was destroyed by NotI digestion, fill in with Klenow fragment, and blunt-end ligation to enable the transposon mutagenesis approach.

Transposon library generation. Using the cDNA clone of DENV strain 16681, pD2/IC-30P-NBX, we created three subgenomic clones by excising the fragments flanked by the unique SacI and NarI sites (A fragment), the unique NarI and EcoRV sites (B fragment), or the unique EcoRV and XbaI sites (C fragment). These three fragments were cloned back into the vector background containing a modified multiple cloning site containing SacI, NarI, EcoRV, and XbaI sites. The MuA transposase (Thermo Fisher) was used to introduce a linear DNA sequence randomly throughout these fragments by the manufacturer's protocol. The linear DNA sequence includes an antibiotic resistance gene flanked by modified inverted repeats of the bacteriophage Mu right-end sequence that have been engineered to contain a NotI site. The mutant A, B, and C fragment libraries were then cloned back into an unmutagenized vector background with antibiotic selection so that the libraries contained only transposons within the DENV genomic fragments and not within the vector backbone. The bulk of the transposon was then excised by performing a NotI restriction enzyme digestion, followed by an intramolecular ligation. This approach resulted in a small, 15-nucleotide genetic scar (underlined) consisting of a NotI site flanked by a T and an A and followed by a duplication of the 5 nucleotides on the 5′ end of the insertions ($N_1N_2N_3N_4N_5$ $\underline{TGCGGCCGCAN_1N_2N_3N_4N_5}$). Colonies with the NotI-containing fragments were pooled, and the plasmid libraries were purified. The colonies were enumerated to estimate the coverage of insertions in the viral genome.

Transposon library selection in Vero cells. Full-length DENV genomes were constructed from each mutagenized A, B, or C fragment library containing the 15-nucleotide site with the remaining wild-type fragments, using SOE PCR with Q5 DNA polymerase (NEB), so that the full-length genome contained only a single insertion. Viral RNA genomes were transcribed *in vitro* using the MEGAscript T7 transcription kit (Thermo Fisher) as previously described (29). Samples of the transcribed input viral RNA libraries were converted to randomly primed cDNA by reverse transcription using the High Capacity cDNA kit (Promega) with the manufacturer's protocol and saved for NGS. *In vitro*-transcribed viral RNAs were

transfected into Vero cells using RNAmessenger transfection reagents (Qiagen) with 2 μg of viral RNA, 4 μl of enhancer reagent, and 8 μl of transfection reagent. The transfection reagent was washed off the cells after 1 h of transfection. To minimize bottleneck effects of the transfection and subsequent passages, transfections were performed in 18 replicates with a total of 36 μg of viral RNA for the A and C fragment libraries and 9 replicates for the B fragment library, with a total of 18 μg of viral RNA. After transfection, the replicates were pooled, and then half of the supernatant was passaged onto naive cells 3 days after transfection. The other half of the supernatant was used to isolate viral RNA using the VR Viral RNA extraction kit (Qiagen). Viral genomes were reverse transcribed as described above, and the concentration was determined with PicoGreen (Thermo Fisher).

NGS library creation. Reverse-transcribed viral genomes from the input library, passage 2, and passage 3 were prepared for amplicon sequencing. Viral cDNA was amplified and fragmented in 28 PCRs into approximately 400-bp amplicons that were prepared for ligation using an end repair kit (NEB), followed by blunt ligation to the P1 Ion Torrent sequencing adaptor on both ends of the PCR product using T4 DNA ligase (NEB). Next, the ligated PCR products were NotI digested and ligated to a modified A Ion Torrent sequencing adaptor containing a NotI sticky end. In this way, only PCR products containing a NotI site should contain both the A and P1 adaptors required for sequencing, and the beginning of each read should be the NotI site followed by the transposon insertion site. The libraries were sequenced by the University of Michigan Sequencing Core using the Ion PGM Hi-Q version 2 sequencing reagents with the 318 chip sets. Input, passage 2, and passage 3 sequencing libraries from each fragment library (A, B, or C) were separately barcoded and sequenced together on the same 318 chip. After demultiplexing the raw reads, the reads were filtered to remove sequencing results lacking a NotI site. The filtered reads were aligned to the viral genome using Bowtie2 with the default settings. Sites in the DENV genome that did not have a mapped read in the input sample but had mapped reads from passage 2 or passage 3 were arbitrarily assigned a value of 0.5 read in the input for further analysis.

DENV propagation. Vero or C6/36 cells (5×10^5) were plated onto 12-well plates. The next day, the cells were infected on ice for 1 h at an MOI of 0.05 PFU/cell. The cells were then washed three times in sterile phosphate-buffered saline (PBS), and fresh medium was placed on the cells. The medium was harvested from the cells at 1, 3, 5, and 7 days postinfection, and the titer was determined by plaque assay as previously described (30).

Western blotting. Whole-cell lysates from Vero, 293T, or C6/36 cells were generated by adding 2× SDS-PAGE sample buffer to the cells and boiling for 5 min. The lysates were separated by SDS-PAGE, and immunoblots were performed as previously described (31). Anti-HA antibody (Cell Signaling; C29F4) was used at a dilution of 1:2,000, the Capsid antibody (Genetex; 103343) was used at a dilution of 1:1,000, the GFP antibody (Cell Signaling; 2956S) was used at a dilution of 1:2,500, and the NS4B antibody (Genetex; 103349) was used at a dilution of 1:1,000 in 5% bovine serum albumin (BSA)/Tris-buffered saline with Tween 20 (TBST) overnight at 4°C. The polyvinylidene difluoride (PVDF) membranes were than washed four times for 5 min each time in TBST. The membranes were incubated in 5% BSA/TBST containing 1:500-diluted secondary antibodies conjugated to horseradish peroxidase (Thermo Fisher) and washed four additional times for 5 min each time. The membranes were then developed using SuperSignal West Femto chemiluminescent substrate (Thermo Fisher) and imaged on a Li-Cor Odyssey.

Immunofluorescence assay. Vero cells (5×10^5) were plated onto a 12-well plate containing sterile glass coverslips. The cells were infected at an MOI of 0.05 PFU/cell on ice for 1 h and washed three times with sterile PBS before fresh medium was applied. At the indicated time points, the cells were fixed in 4% paraformaldehyde in PBS for 10 min at room temperature. The cells were washed briefly in PBS and blocked for 30 min in PBS–10% fetal bovine serum–0.1% Triton X-100. The cells were then incubated with primary antibodies for 1 h in blocking solution, washed four times with PBS, incubated with a secondary antibody diluted in blocking solution, and washed an additional four times. The cells were mounted onto glass slides using Prolong Gold Antifade reagent without DAPI (4′,6-diamidino-2-phenylindole) (Thermo Fisher). The slides were imaged at the University of Michigan Microscope and Image Analysis Laboratory using a Nikon A-1 confocal microscope.

Sanger sequencing of the DENV genome. *In vitro*-transcribed viral RNAs were transfected into 293T cells using the RNAmessenger transfection reagents (Qiagen) as described above. Seven days posttransfection, random-primed cDNA was prepared from the cell culture supernatant, as described above. cDNA samples were PCR amplified, gel purified, and submitted to Sanger sequencing at the University of Michigan DNA Sequencing Core. In addition, cell culture supernatant from the original transfection was propagated on naive 293T cells for 5 days and passaged in this manner three consecutive times. All four passages were analyzed as described above. Chromatographs were visualized using Codoncode Aligner (Codoncode Corp.).

Dengue viral RNA quantitation by qPCR. Cell-free viral RNA was harvested at the indicated times, and random-primed cDNA was prepared as described above. cDNA preparations were analyzed by quantitative PCR (qPCR) using Fast SYBR master mix (Invitrogen) in a CFX Connect real-time qPCR system (Bio-Rad). For absolute quantification of viral genomes, a standard curve was established using 10-fold dilutions of the plasmid carrying the dengue virus serotype 2 strain 16881 cDNA ranging from 4.3×10^2 to 4.3×10^8 copies. Previously published sense and antisense primers were complementary to a conserved region of NS1 (sense sequence, 5′-AAAGTCACACACTCTATGGAGCAATG-3′; antisense sequence, 5′-GTGGTTGTTCTTAAAGAGGGTCCTC-3′) (32). For cellular RNA experiments, human β-actin primers were used for relative quantitation of dengue viral genomes using $\Delta\Delta C_T$ analysis (human β-actin sense sequence, 5′-AAGTGTGACGTTGACATCCG-3′, and antisense sequence, 5′-GATCCACATCTGCTGGAAGG-3′).

Dengue virus propagation. *In vitro*-transcribed viral RNAs were transfected into 293T cells as described above. Seven days after transfection, qPCR was used to determine viral genome concentrations. Naive cells were infected at an MOI of 1 genome per cell for 4 h at 37°C, and media were replaced. Five days after infection, total cellular RNA was harvested, and viral genomes were determined by qPCR as described above.

Dengue viral RNA protection assay. Cell culture supernatants were subjected to 250 U of Pierce Universal Nuclease (Thermo Fisher) in the presence or absence of 1% NP-40 for 4 h at 37°C. *In vitro*-transcribed RNA was used as a control. The Pierce Universal Nuclease was inactivated by the β-mercaptoethanol present in the lysis buffer of the VR viral RNA preparation kit (Qiagen), and viral RNA was isolated and quantitated by qRT-PCR as described above.

Dengue virus capsid *trans*-complementation. *In vitro*-transcribed viral RNAs were transfected into 293T cells as described above. One day after transfection, a plasmid encoding full-length DENV Capsid or enhanced GFP (eGFP) was transfected into the cells using Fugene HD (Promega) according to the manufacturer's recommendations. Seven days after transfection, qRT-PCR was used to determine viral genome concentrations in cell-free supernatant. Naive 293T cells were infected at an MOI of 1 genome/cell for 4 h at 37°C, and the medium was replaced. Five days after infection, total cellular RNA was harvested, and viral genomes were determined by qRT-PCR as described above.

Statistics. Statistical analysis was performed using Prism software v 6.1 (Graphpad Software). A two-tailed Student *t* test was used to determine statistical significance.

SUPPLEMENTAL MATERIAL

Supplemental material for this article may be found at https://doi.org/10.1128/JVI.02085-17.

SUPPLEMENTAL FILE 1, XLSX file, 0.6 MB.

ACKNOWLEDGMENTS

We have no conflicts of interest to disclose.

We thank Claire Huang (CDC) for the pD2/IC-30-P-NBX infectious cDNA clone and David Akey (University of Michigan) for help with the three-dimensional (3D) models of Capsid and NS5.

This work was supported by National Institutes of Health grant R01DK097374 (A.W.T.), Michigan Institute for Clinical and Health Research (MICHR) grant UL1TR002240 (J.W.P.), and University of Michigan Center for Gastrointestinal Research (UMCGR) grant 5P30DK034933.

REFERENCES

1. Bhatt S, Gething PW, Brady OJ, Messina JP, Farlow AW, Moyes CL, Drake JM, Brownstein JS, Hoen AG, Sankoh O, Myers MF, George DB, Jaenisch T, Wint GR, Simmons CP, Scott TW, Farrar JJ, Hay SI. 2013. The global distribution and burden of dengue. Nature 496:504–507. https://doi.org/10.1038/nature12060.
2. Brady OJ, Gething PW, Bhatt S, Messina JP, Brownstein JS, Hoen AG, Moyes CL, Farlow AW, Scott TW, Hay SI. 2012. Refining the global spatial limits of dengue virus transmission by evidence-based consensus. PLoS Negl Trop Dis 6:e1760. https://doi.org/10.1371/journal.pntd.0001760.
3. Guzmán MG, Kouri G. 2002. Dengue: an update. Lancet Infect Dis 2:33–42. https://doi.org/10.1016/S1473-3099(01)00171-2.
4. Gubler DJ. 2004. The changing epidemiology of yellow fever and dengue, 1900 to 2003: full circle? Comp Immunol Microbiol Infect Dis 27:319–330. https://doi.org/10.1016/j.cimid.2004.03.013.
5. Guzman MG, Halstead SB, Artsob H, Buchy P, Farrar J, Gubler DJ, Hunsperger E, Kroeger A, Margolis HS, Martinez E, Nathan MB, Pelegrino JL, Simmons C, Yoksan S, Peeling RW. 2010. Dengue: a continuing global threat. Nat Rev Microbiol 8(12 Suppl):S7–S16. https://doi.org/10.1038/nrmicro2460.
6. Guy B, Briand O, Lang J, Saville M, Jackson N. 2015. Development of the Sanofi Pasteur tetravalent dengue vaccine: one more step forward. Vaccine 33:7100–7111. https://doi.org/10.1016/j.vaccine.2015.09.108.
7. Villar L, Dayan GH, Arredondo-García JL, Rivera DM, Cunha R, Deseda C, Reynales H, Costa MS, Morales-Ramírez JO, Carrasquilla G, Rey LC, Dietze R, Luz K, Rivas E, Miranda Montoya MC, Cortés Supelano M, Zambrano B, Langevin E, Boaz M, Tornieporth N, Saville M, Noriega F. 2015. Efficacy of a tetravalent dengue vaccine in children in Latin America. N Engl J Med 372:113–123. https://doi.org/10.1056/NEJMoa1411037.
8. Capeding MR, Tran NH, Hadinegoro SRS, Ismail HI, Chotpitayasunondh T, Chua MN, Luong CQ, Rusmil K, Wirawan DN, Nallusamy R, Pitisuttithum P, Thisyakorn U, Yoon I-K, van der Vliet D, Langevin E, Laot T, Hutagalung Y, Frago C, Boaz M, Wartel TA, Tornieporth NG, Saville M, Bouckenooghe A. 2014. Clinical efficacy and safety of a novel tetravalent dengue vaccine in healthy children in Asia: a phase 3, randomised, observer-masked, placebo-controlled trial. Lancet 384:1358–1365. https://doi.org/10.1016/S0140-6736(14)61060-6.
9. Aguiar M, Stollenwerk N, Halstead SB. 2016. The impact of the newly licensed dengue vaccine in endemic countries. PLoS Negl Trop Dis 10:e0005179. https://doi.org/10.1371/journal.pntd.0005179.
10. Ferguson NM, Rodríguez-Barraquer I, Dorigatti I, Mier-y-Teran-Romero L, Laydon DJ, Cummings DAT. 2016. Benefits and risks of the Sanofi-Pasteur dengue vaccine: modeling optimal deployment. Science 353:1033. https://doi.org/10.1126/science.aaf9590.
11. Acosta EG, Kumar A, Bartenschlager R. 2014. Revisiting dengue virus-host cell interaction. Adv Virus Res 88:1–109. https://doi.org/10.1016/B978-0-12-800098-4.00001-5.
12. Chatel-Chaix L, Bartenschlager R. 2014. Dengue virus- and hepatitis C virus-induced replication and assembly compartments: the enemy inside-caught in the web. J Virol 88:5907–5911. https://doi.org/10.1128/JVI.03404-13.
13. Lin C, Amberg SM, Chambers TJ, Rice CM. 1993. Cleavage at a novel site in the NS4A region by the yellow fever virus NS2B-3 proteinase is a prerequisite for processing at the downstream 4A/4B signalase site. J Virol 67:2327–2335.
14. Byk LA, Gamarnik AV. 2016. Properties and functions of the dengue virus capsid protein. Annu Rev Virol 3:263–281. https://doi.org/10.1146/annurev-virology-110615-042334.
15. Chalker JM, Bernardes GJL, Davis BG. 2011. A "tag-and-modify" approach to site-selective protein modification. Acc Chem Res 44:730–741. https://doi.org/10.1021/ar200056q.

16. Herod MR, Loundras E-A, Ward JC, Tulloch F, Rowlands DJ, Stonehouse NJ. 2015. Employing transposon mutagenesis to investigate foot-and-mouth disease virus replication. J Gen Virol 96:3507–3518. https://doi.org/10.1099/jgv.0.000306.
17. Thorne L, Bailey D, Goodfellow I. 2012. High-resolution functional profiling of the norovirus genome. J Virol 86:11441–11456. https://doi.org/10.1128/JVI.00439-12.
18. Beitzel BF, Bakken RR, Smith JM, Schmaljohn CS. 2010. High-resolution functional mapping of the Venezuelan equine encephalitis virus genome by insertional mutagenesis and massively parallel sequencing. PLoS Pathog 6:e1001146. https://doi.org/10.1371/journal.ppat.1001146.
19. Arumugaswami V, Remenyi R, Kanagavel V, Sue EY, Ngoc Ho T, Liu C, Fontanes V, Dasgupta A, Sun R. 2008. High-resolution functional profiling of hepatitis C virus genome. PLoS Pathog 4:e1000182. https://doi.org/10.1371/journal.ppat.1000182.
20. Remenyi R, Qi H, Su S-Y, Chen Z, Wu NC, Arumugaswami V, Truong S, Chu V, Stokelman T, Lo H-H, Olson CA, Wu T-T, Chen S-H, Lin C-Y, Sun R. 2014. A comprehensive functional map of the hepatitis C virus genome provides a resource for probing viral proteins. mBio 5:e01469–14. https://doi.org/10.1128/mBio.01469-14.
21. Fulton BO, Sachs D, Schwarz MC, Palese P, Evans MJ. 2017. Transposon mutagenesis of the zika virus genome highlights regions essential for RNA replication and restricted for immune evasion. J Virol 91:e00698–17. https://doi.org/10.1128/JVI.00698-17.
22. Miller S, Kastner S, Krijnse-Locker J, Bühler S, Bartenschlager R. 2007. The non-structural protein 4A of dengue virus is an integral membrane protein inducing membrane alterations in a 2K-regulated manner. J Biol Chem 282:8873–8882. https://doi.org/10.1074/jbc.M609919200.
23. Shrivastava G, García-Cordero J, León-Juárez M, Oza G, Tapia-Ramírez J, Villegas-Sepulveda N, Cedillo-Barrón L. 2017. NS2A comprises a putative viroporin of Dengue virus 2. Virulence 8:1450–1456. https://doi.org/10.1080/21505594.2017.1356540.
24. Sangiambut S, Suphatrakul A, Sriburi R, Keelapang P, Puttikhunt C, Kasinrerk W, Malasit P, Sittisombut N. 2013. Sustained replication of dengue pseudoinfectious virus lacking the capsid gene by trans-complementation in capsid-producing mosquito cells. Virus Res 174:37–46. https://doi.org/10.1016/j.virusres.2013.02.009.
25. Teoh P-G, Huang Z-S, Pong W-L, Chen P-C, Wu H-N. 2014. Maintenance of dimer conformation by the dengue virus core protein α4-α4′ helix pair is critical for nucleocapsid formation and virus production. J Virol 88:7998–8015. https://doi.org/10.1128/JVI.00940-14.
26. Chatel-Chaix L, Fischl W, Scaturro P, Cortese M, Kallis S, Bartenschlager M, Fischer B, Bartenschlager R. 2015. A combined genetic-proteomic approach identifies residues within dengue virus NS4B critical for interaction with NS3 and viral replication. J Virol 89:7170–7186. https://doi.org/10.1128/JVI.00867-15.
27. Chatel-Chaix L, Cortese M, Romero-Brey I, Bender S, Neufeldt CJ, Fischl W, Scaturro P, Schieber N, Schwab Y, Fischer B, Ruggieri A, Bartenschlager R. 2016. Dengue virus perturbs mitochondrial morphodynamics to dampen innate immune responses. Cell Host Microbe 20:342–356. https://doi.org/10.1016/j.chom.2016.07.008.
28. Eyre NS, Johnson SM, Eltahla AA, Aloi M, Aloia AL, McDevitt CA, Bull RA, Beard MR. 2017. Genome-wide mutagenesis of dengue virus reveals plasticity of the NS1 protein and enables generation of infectious tagged reporter viruses. J Virol 91:e01455–17. https://doi.org/10.1128/JVI.01455-17.
29. Prestwood TR, Prigozhin DM, Sharar KL, Zellweger RM, Shresta S. 2008. A mouse-passaged dengue virus strain with reduced affinity for heparan sulfate causes severe disease in mice by establishing increased systemic viral loads. J Virol 82:8411–8421. https://doi.org/10.1128/JVI.00611-08.
30. Roehrig JT, Hombach J, Barrett ADT. 2008. Guidelines for plaque-reduction neutralization testing of human antibodies to dengue viruses. Viral Immunology 21:123–132. https://doi.org/10.1089/vim.2008.0007.
31. Perry JW, Wobus CE. 2010. Endocytosis of murine norovirus 1 into murine macrophages is dependent on dynamin II and cholesterol. J Virol 84:6163–6176. https://doi.org/10.1128/JVI.00331-10.
32. Yenchitsomanus PT, Jaruthasana I, Pattanakitsakul SN, Nitayaphan S, Mongkolsapaya J, Malasit P. 1996. Rapid detection and identification of dengue viruses by polymerase chain reaction (PCR). Southeast Asian J Trop Med Public Health 27:228–236.